nature communications

Article

https://doi.org/10.1038/s41467-025-67404-1

Symbiosome functionality in *Medicago truncatula* nodules requires continuous clearing of pectins from the symbiosome space

Received: 25 February 2025

Accepted: 28 November 2025

Published online: 13 December 2025

Check for updates

Yongkang Gao[1,5], Lei Chen[1,5], Wei Yang[1], Tong Yue[1], Qianqian Li[1], Kuan Chen[1], Jing Yuan[2], Xia Li[1], Thomas Ott[3,4] ✉ & Chao Su[1] ✉

Central to the legume–rhizobium symbiosis is the formation of organelle-like symbiosomes where nitrogen-fixing bacteroids are enclosed by a host-derived symbiosome membrane. This creates the symbiosome space, which topologically resembles an apoplastic compartment within the cell. While the apoplast of plant cells is largely occupied by the cell wall, symbiosomes are devoid of cell wall polymers. Here, we describe a mechanism that functions to protect and maintain effective nitrogen fixation through the action of cell-wall-degrading enzymes that prevent accumulation of un-esterified pectin within symbiosomes. We identify two symbiotically-induced polygalacturonase (PG) genes in *Medicago truncatula*, *SyPG1* and *SyPG2*, that are secreted into the symbiosome space. Silencing the expression of *SyPG1/2* or editing *SyPG1/2* via CRISPR-Cas9 both lead to nodule senescence and trigger excessive accumulation of un-esterified pectin in symbiosome containing cells. Additionally, we show that un-esterified pectins inhibit rhizobial growth both in vivo and in vitro. Together, our results provide evidence for a host-controlled cell wall clearance mechanism that is essential for symbiosome maintenance.

Plant cells are surrounded by a cell wall (CW), that maintains cell shape and integrity. The composition of the CW not only differs between plant lineages but also strongly depends on cell age, organ identity and extracellular stimuli[1]. The main components are cellulose, hemicelluloses, pectins, and structural proteins with pectins being highly abundant in young and more flexible cell walls. Pectins comprise a complex group of polysaccharides that includes homogalacturonan (HG), xylogalacturonan, apiogalacturonan, rhamnogalacturonan I (RG-I), and rhamnogalacturonan II (RG-II), with HG being the most abundant and extensively studied form ref. 2. Pectin biosynthesis occurs in the Golgi apparatus, where it is produced in a highly methylesterified form and subsequently secreted into the apoplast and integrated into the cell wall[3]. There, pectin methylesterases (PMEs) catalyze the removal of methyl groups from HG, generating regions of de-esterified pectin[4,5]. These de-esterified regions can either interact with calcium ions to form gel-like cross-linked networks or serve as substrates for pectin-degrading enzymes such as pectate lyase (PL) and polygalacturonase (PG)[6]. Through these enzymatic modifications, the structure and function of the cell wall are dynamically regulated during plant growth, development, and stress responses.

Serving as a physical barrier against pathogenic bacteria and fungi, micro-organisms have to actively overcome the cell wall to

[1]National Key Laboratory of Crop Genetic Improvement, College of Plant Science and Technology, Huazhong Agricultural University, Hubei Hongshan Laboratory, Wuhan, China. [2]National Key Laboratory of Agricultural Microbiology, Huazhong Agricultural University, Wuhan, China. [3]Faculty of Biology, University of Freiburg, Freiburg, Germany. [4]CIBSS – Centre of Integrative Biological Signalling Studies, University of Freiburg, Freiburg, Germany. [5]These authors contributed equally: Yongkang Gao, Lei Chen. ✉e-mail: thomas.ott@biologie.uni-freiburg.de; chaosu@mail.hzau.edu.cn

invade cells and tissues. To achieve this, they secrete a cocktail of cell wall degrading enzymes, including PLs, PGs, pectin lyases, hemicellulases and cellulases[7]. This situation may be inverted during symbiotic associations, such as the interaction between legumes and rhizobia when establishing the root nodule symbiosis. During this mutualistic bacteria-plant interaction, symbiotic rhizobia colonize legumes, and some other species mostly via root hairs, where the host initiates the formation of a membrane tunnel called the infection thread (IT)[8]. These invasively and polarly growing membrane structures progress transcellularly through the root cortex and branch in the developing nodule primordium, where bacteria are released into specialized cells[8]. The transcellular passage requires significant cell wall modifications at the cell-cell interface leading to the formation of the transcellular passage cleft[9]. Bacteria are released from ITs at specialized sites, called "infection droplets" that are devoid of a cell wall and may instead be stabilized by the symbiotic remorin protein SYMREM1[10]. While rhizobia bud off from the droplet in a endocytosis-like process, they are and remain surrounded by a host derived membrane called the "symbiosome membrane" (SM). Depending on the plant species single or few bacteria are encapsulated in the SM where they differentiate into nitrogen-fixing bacteroids that deliver fixed nitrogen via the SM to the host cell. In return, the host provides photosynthetic sugars to the symbiont. Different to the above-described interactions, infected nodule cells are filled with thousands of independent symbiosomes that are entirely detached from the host membrane and are maintained as cell wall free compartments throughout their entire life span. Taking pectins as an example, it has been shown that methylesterified pectins accumulate in the cell periphery of infected nodule cells but not within ITs, while demethylesterified pectins were mainly found in the cell wall structure of ITs[11]. This finding was explained with the continuous activity of PMEs and the spatio-temporally restricted presence of the nodule pectate lyase NPL[11]. None of these pectin forms has, however, been detected in the symbiosome space, the area in between the SM and the bacterial surface, that is devoid of a plant cell wall[11]. So far, it has been hypothesized that upon bacterial release from cell wall-free infection droplets, symbiosomes remain devoid of cell wall components[12,13]. However, data from *Pisum sativum* suggest that RG-II accumulates to some extent in the symbiosome space of young symbiosomes with undifferentiated bacteroids, while it is depleted with increasing symbiosome age[14]. This could be explained in two different ways: First, pectin biosynthesis and secretion are entirely abolished in mature infected cells or second, that symbiosomes contain pectin-degrading enzymes that continuously remove pectins secreted into the symbiosome space. Here, we show evidence for the latter pathway and demonstrate that at least two polygalacturonases are required to continuously clear the symbiosome space from pectin accumulation.

Results

A nodule PME is enriched in the symbiosome space

Symbiosomes as the nitrogen-fixing organelles, lack a robust cell wall. In line with this, they neither accumulate pectins nor xyloglucans[11]. However, esterified pectins and xyloglucans do accumulate in the peripheral cell wall of infected cells[11]. This implies that although esterified pectin synthesis is persistent in these cells, they may be continuously cleared from the symbiosome space. This process would require the action of PLs or PGs as PME-driven de-esterification of secreted pectins is a pre-requisite of PL-/PG-mediated pectin degradation. Indeed, a symbiotic PME (SyPME) was reported to be induced by rhizobia inoculation and required for IT growth in *Medicago truncatula* (hereafter *M. truncatula*)[11]. This work also pointed to the presence of another PME (*Medtr2g105560*), which shows highest expression in nodules with a predominant enrichment in the nodule infection zone[11]. Thus, we named it nodule PME (nPME). To assess pectin dynamics in symbiosomes, we first monitored the presence of SyPME and nPME. While the previously described SyPME protein accumulated around ITs and in intercellular spaces in the infection zone of indeterminate *M. truncatula* nodules (Supplementary Fig. 1a–a")[11], nPME was strongly enriched in the symbiosome space at the interzone of *M. truncatula* nodules (Fig. 1a–d and Supplementary Fig. 2) but not in the cell periphery and ITs (Fig. 1e–e"). This indicates that active pectin de-esterification inside the symbiosome space is maintained and further supports the hypothesis that pectins are continuously cleared from this compartment.

Rhizobia-induced symbiotic *PG*s accumulate in the symbiosome space

To test the above hypothesis, we first confirmed that NPL does not accumulate around symbiosomes but rather localizes around nodular ITs and strongly accumulates at cell wall-less infection droplets as suggested earlier (Supplementary Fig. 1b–b")[11]. As PGs provide an alternative path for pectin degradation, we selected candidate *PGs* based on their expression profiles using publicly available transcriptomic data[15,16]. Of the 80 *PG* genes annotated in the *M. truncatula* genome (Supplementary Fig. 3), expression profiles of 56 *PGs* could be retrieved from *M. truncatula* nodule transcriptomic data[15,17]. Based on these profiles, six *PGs* (*Medtr4g094715*, *Medtr8g028725*, *Medtr6g028080*, *Medtr8g098840*, *Medtr2g032710*, and *Medtr7g078680*) were initially selected as they were highly transcribed in nodules with their expression being restricted to either the infection zone or interzone of *M. truncatula* nodules (Supplementary Data 1 and Supplementary Fig. 4a). Among the six selected *PG*s, two of them are dependent on EFD (Supplementary Data 1 and Supplementary Fig. 4b), a key transcription factor that regulates rhizobial release and differentiation[18]. Thus, we re-named *Medtr2g032710* and *Medtr6g028080* as *SyPG1* (*Symbiotic PG1*) and *SyPG2*, respectively.

To verify the expression patterns and to gain more cellular resolution, we generated promoter-GUS reporter constructs for *SyPG1* and *SyPG2* by using 2 kb upstream of their transcriptional start sites. Roots transformed with these reporter constructs were inoculated for two weeks with *Sinorhizobium meliloti* 2011 (hereafter *S. meliloti* 2011) before promoter activity was visualized based on β-glucuronidase (GUS) activity. Both *SyPG1* and *SyPG2* reporters showed activity in nodule primordia and within the vascular bundle of the root (Supplementary Fig. 5a, b), while staining was more restricted to the apical region (meristematic zone and infection zone) of mature nodules (Supplementary Fig. 5c, d). We additionally conducted in situ hybridization experiments to localize the respective mRNAs in nodule tissues. The transcripts of *SyPG1* and *SyPG2* both exhibited expression in nodule primordia (Supplementary Fig. 5e–l). Notably, the accumulation of *SyPG1* and *SyPG2* transcripts were predominantly detected within the interzone of mature nodules (Supplementary Fig. 5m–p). Given the dominant promoter activity in the meristematic and infection zone, it is hypothesized that the promoter sequence employed may be lacking in specific *cis*-elements necessary for the expression of those genes. Notably, it is also possible that the transcripts of those genes are either stabilized during cell differentiation and maturation in the nodule or that the corresponding mRNAs exhibit a certain extent of transcellular mobility.

To elucidate the subcellular patterning of the SyPG1 and SyPG2 proteins, we examined their localization in nodule cells by expressing SyPG1/2-GFP fusion proteins using a hairy root transformation system. For SyPG1, we observed distinct fluorescence along nodular ITs and in infection droplets, where bacteria are released into host cells (Supplementary Fig. 6a, b). By contrast, no SyPG2-GFP signal was detected around these sites (Supplementary Fig. 6c, d). Unexpectedly, we found comparably strong and symbiosome-confined accumulations of both SyPG1-GFP and SyPG2-GFP in infected cells of the nodule interzone (Fig. 2 and Supplementary Fig. 7), resembling the patterns observed for nPME (Fig. 1a–d). Thus, these data further strengthen the

https://doi.org/10.1038/s41467-025-67404-1

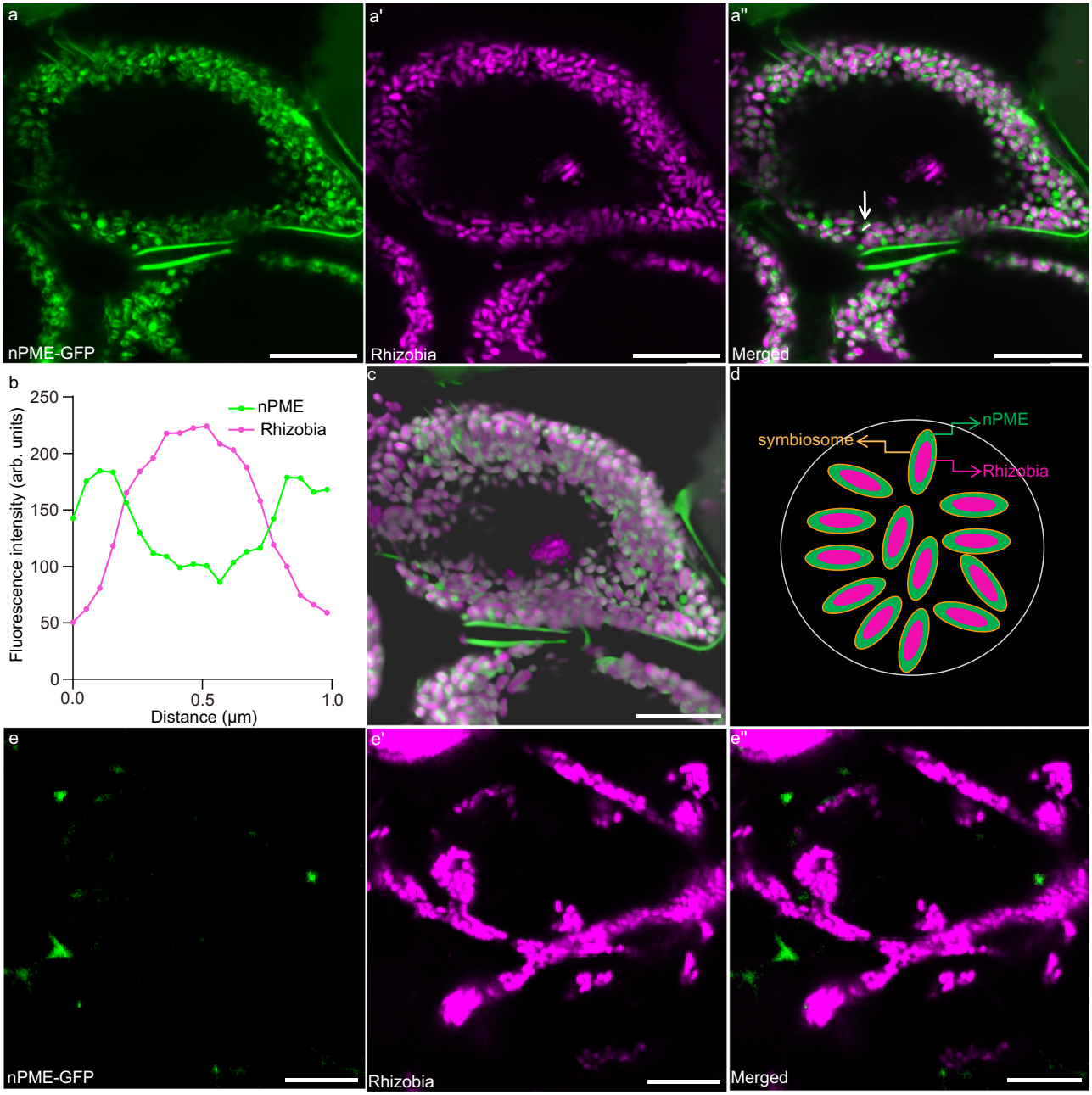

Fig. 1 | nPME is located in the symbiosome space. Confocal images of 14 days old nodules embedded in agarose and sectioned. **a**–**a″** nPME is located within symbiosomes in infected cells (IC) of the nodule interzone ($n = 20$ nodules). **b** Fluorescence intensities were measured along the region marked with white line and white arrow in (**a″**). Fluorescence intensity measurements were performed with Fiji, and graphs were generated with GraphPad Prism 10. **c**, **d** The localization of nPME-GFP is shown as a 3D projection generated by using Imaris (**c**) and the sketch was drawn using Adobe Illustrator (**d**). **e**–**e″** nPME does not accumulate along nodular ITs ($n = 20$ nodules). The experiment was conducted with 3 independent replicates, each involving analysis of at least 20 nodules. Green indicates the GFP-tagged nPME signal and magenta indicates the mCherry-tagged *S. meliloti* 2011. Scale bars = 10 µm.

hypothesis that the symbiosome space is actively cleared from pectin material.

Knock-down the expression of *SyPG1/2* leads to nodule senescence

To genetically assess whether SyPGs are important for nodule function, we cloned an RNA interference (RNAi) construct to simultaneously knock down the expression of both *SyPG1* and *SyPG2*. Indeed, expression analysis of *SyPG1* and *SyPG2* transcripts in transgenic roots expressing the RNAi construct (*SyPG1/2-RNAi*) and being inoculated for 3 weeks with *S. meliloti* 2011 confirmed a significant reduction of both transcripts (Fig. 3a, b and Supplementary Fig. 8). The analysis of expression levels for the initially selected four other *PGs* indicated that only the transcripts of *Medtr8g098840* were targeted by the *SyPG1/2-RNAi* construct. In contrast, transcript levels of the remaining three *PGs* exhibited a slight decrease, yet this reduction was not statistically significant (Supplementary Fig. 9). Phenotypically, no significant reduction in overall nodule number was observed at 3 wpi when comparing control plants carrying an empty vector (EV) with *SyPG1/2* knockdown plants (Fig. 3c). We also checked IT growth at the 10 days post-inoculation, without any significant morphological differences being detected between EV and *SyPG1/2* knockdown plants

https://doi.org/10.1038/s41467-025-67404-1

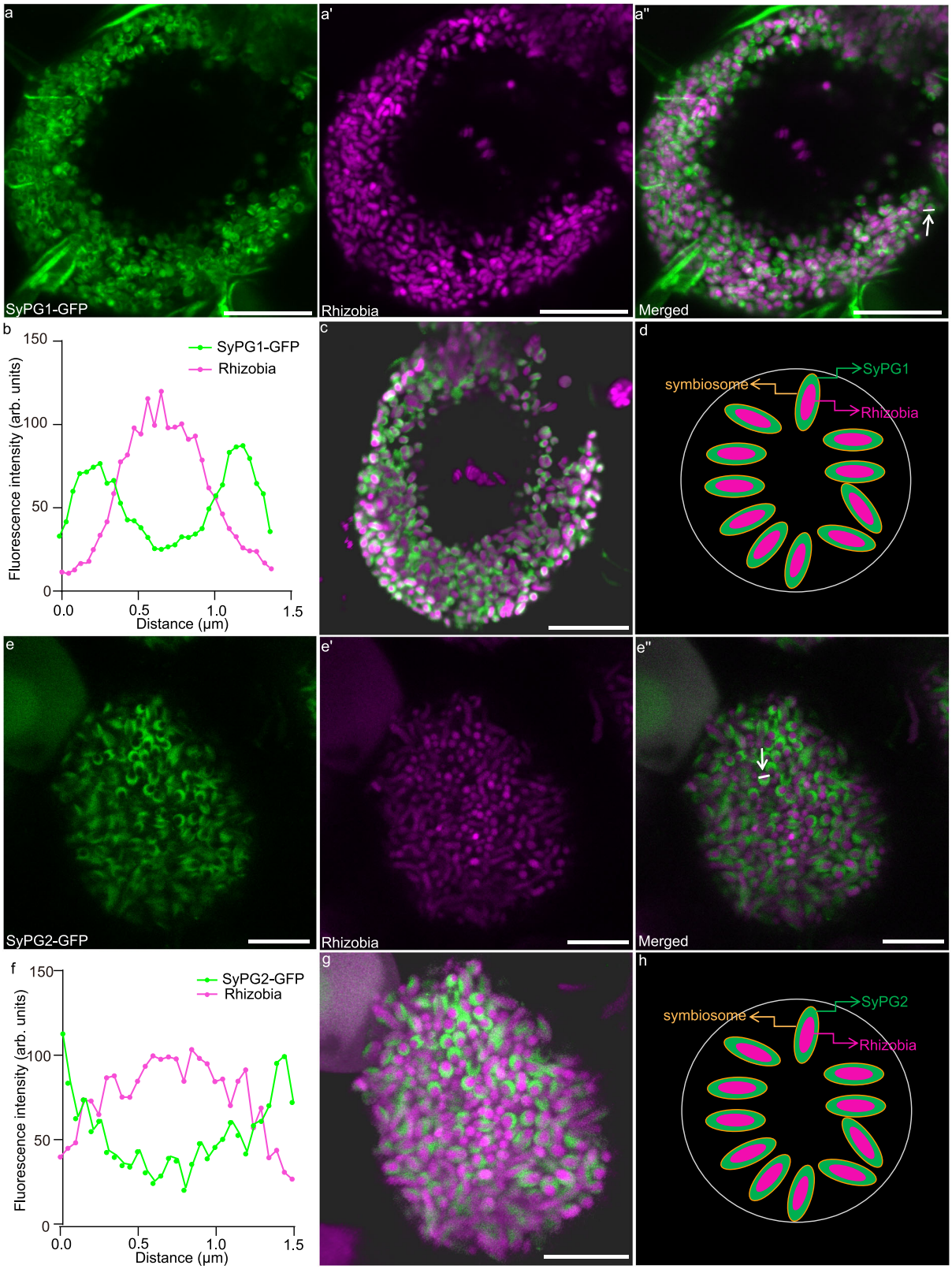

Fig. 2 | SyPG1 and SyPG2 are located in the symbiosome space. Confocal images of 14 days old nodules embedded in agarose and sectioned. **a**–**h** In infected cells within the nodule interzone, both SyPG1 (**a**–**d**) and SyPG2 (**e**–**h**) are located in the symbiosome space surrounding nitrogen-fixing bacteroids ($n \geq 20$ nodules). Graphs in (**b**) and (**f**) display profiles of fluorescence intensities measured along the linear transect marked with white line and white arrow in (**a″**) and (**e″**), respectively. Fluorescence intensity measurements were performed with Fiji, and graphs were generated with GraphPad Prism 10. In (**c**) and (**g**), the localization of SyPG1-GFP (**c**) and SyPG2-GFP (**g**) are shown as 3D projections generated using Imaris. **d** and **h** show the corresponding sketches, which were created using Adobe Illustrator. The subcellular localization of SyPG1 and SyPG2 was analyzed by 3 independent experiments, minimum of 20 nodules were analyzed in each repeat. Green indicates the GFP-tagged SyPG1 and SyPG2 signal and magenta indicates the mCherry-tagged *S. meliloti* 2011. Scale bars = 10 μm.

https://doi.org/10.1038/s41467-025-67404-1

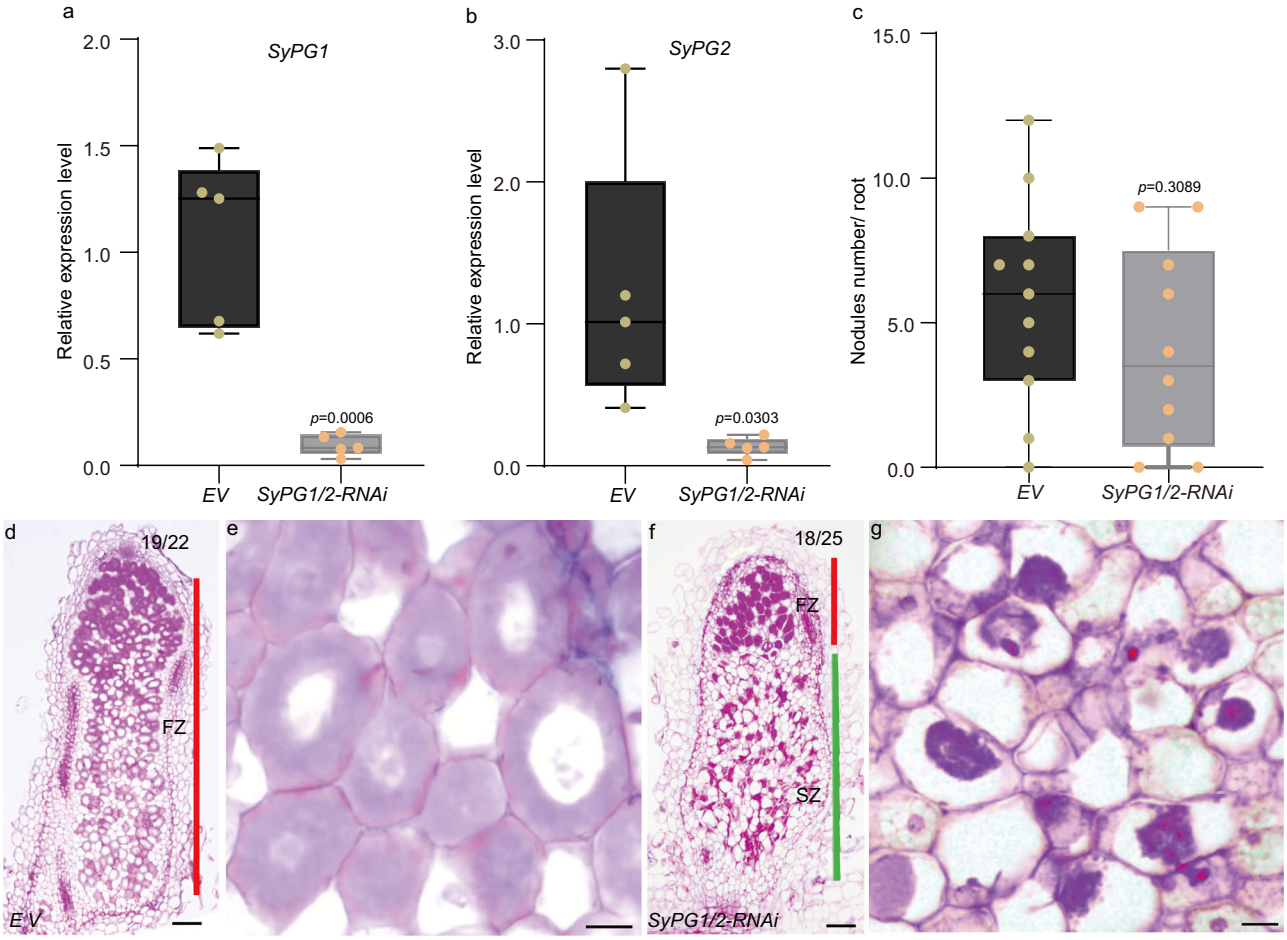

Fig. 3 | The senescence zone is significantly enlarged in *SyPG1/2-RNAi* nodule. **a**, **b** qRT-PCR was used to detect the expression level of *SyPG1* (**a**), *SyPG2* (**b**) in EV and *SyPG1/2-RNAi* transformed roots ($n = 5$ plants) at 21 dpi. **c** The number of nodules in EV ($n = 11$ plants) and *SyPG1/2-RNAi* ($n = 10$ plants) transformed roots was scored at 21 days post-inoculation (dpi). The graphs were generated using GraphPad Prism 10. Box-whiskers plot with all data points shown; the boxes are extended from the 25th to 75th percentiles and the line in the middle of the box is plotted at the median. Data are mean ± SE. Statistics were performed using an unpaired two-tailed student's *t*-test: **a** $p = 0.0006$, **b** $p = 0.0303$, **c** $p = 0.3089$. **d**–**g** Microscopic images of 21 days old nodules embedded in Technovit 7100 and sectioned. Nodules from EV (**d**, **e**, $n = 22$ nodules) and *SyPG1/2-RNAi* (**f**, **g**, $n = 25$ nodules) transformed nodules were embedded in Technovit 7100 and sections were stained with ruthenium red. FZ fixation zone (red bar), SZ senescence zone (green bar). The experiments were performed with 3 independent replicates, each involving a minimum of 20 nodules. Scale bars = 100 µm in (**d**, **f**) and 20 µm in (**e**, **g**).

(Supplementary Fig. 10a, b). Further examination of the nodule structure revealed that the majority of nodules (19/22) from control plants exhibited a large nitrogen-fixing zone (FZ) with a limited senescence zone (SZ; Fig. 3d, e). In contrast, post-transcriptional gene silencing of *SyPG1/2* resulted in nodules (18/25) with a drastically reduced nitrogen-FZ and an expanded SZ compared to the controls (Fig. 3f, g). Given that SyPG1 is also located at the ITs and infection droplets, we further examined ITs in the nodule infection zone of *SyPG1/2* knockdown plants. However, no obvious morphological differences in the ITs between the control plants and the *SyPG1/2* knockdown plants (Supplementary Fig. 10c–f).

To obtain more robust genetic evidence substantiating the function of SyPG1/2, we also utilized CRISPR/Cas9-mediated gene editing, specifically targeting *SyPG1* and *SyPG2* (*SyPG1/2-Cas9*). Sequencing analysis indicated that the roots transformed with *SyPG1/2-Cas9* led to the premature termination of both SyPG1 and SyPG2 (Supplementary Fig. 11a). Subsequently, expression analysis suggested that it had no effect on the expression of other tested *PG* genes (Supplementary Fig. 11b–e). Phenotypic analysis of the nodules from *SyPG1/2-Cas9* transformed plants revealed a similar phenotype, characterized by an enlarged SZ (Supplementary Fig. 11f–i). Those suggest that SyPG1/2 play a positive role in the maintenance of active symbiosome during symbiotic nitrogen fixation.

Un-esterified pectin is enriched around symbiosome in *SyPG1/2-RNAi* nodules

Given the role of PG in pectin degradation, we hypothesized that the down-regulation and/or loss of SyPG1 and SyPG2 in the symbiosome space may result in pectin accumulation within this compartment. To test this, we performed immunofluorescence assays using the LM19 antibody, which recognizes de-esterified pectins, the substrate of PGs. As shown before ref. 11, we confirmed that no reliable LM19 signal can be found in symbiosomes (Fig. 4a, b) of control nodules. By contrast, *SyPG1/2-RNAi* nodules strongly and significantly accumulated de-esterified pectins within infected cells (Fig. 4c–e). To gain resolution, we also applied transmission electron microscopy (TEM) to image the structure of symbiosomes and analysed LM19 signal deposition using an immuno-gold assay. Symbiosomes in infected cells of control (EV) nodules were highly organized with bacteroids displaying homogenous patterns (Fig. 4f, g). In contrast, symbiosomes in *SyPG1/2* knock-down nodules were distorted with the SM only being loosely aligned with the bacteroids (Fig. 4h, i). Consistent with our

https://doi.org/10.1038/s41467-025-67404-1

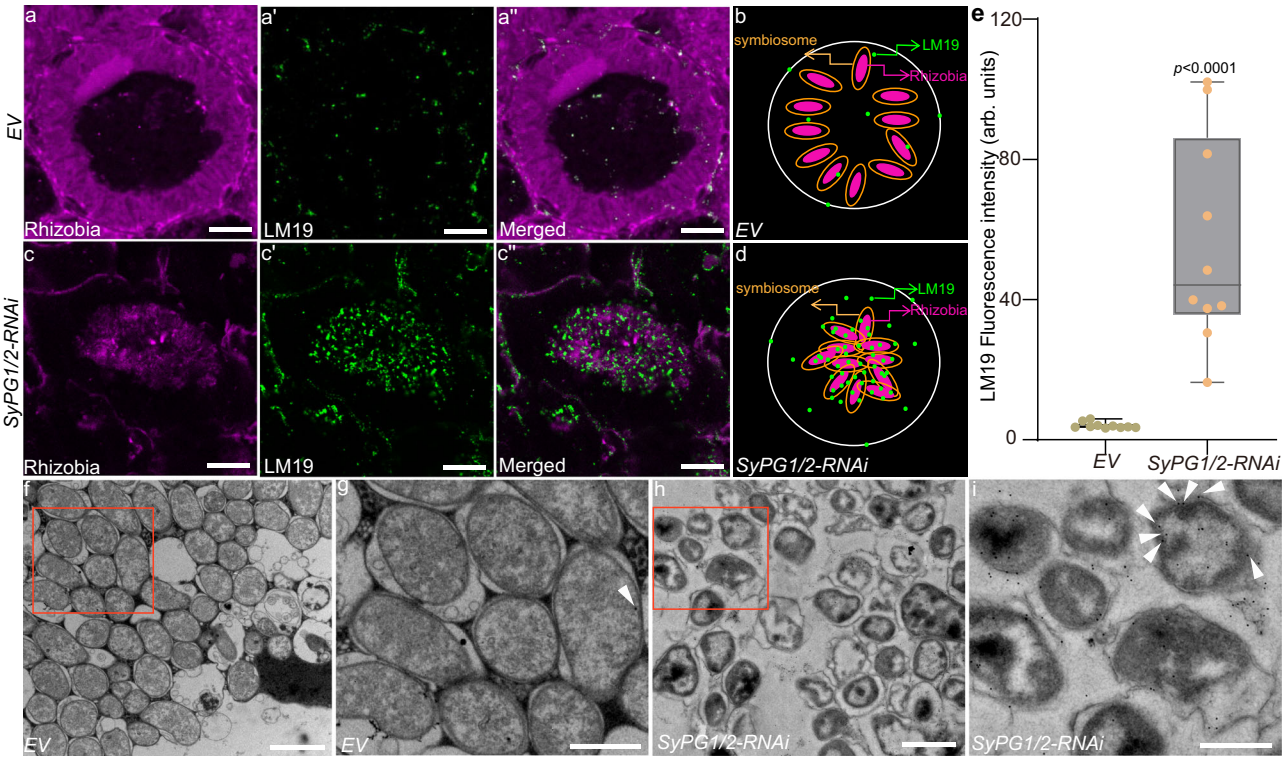

Fig. 4 | Un-esterified pectins accumulate within symbiosomes in *SyPG1/2-RNAi* nodules. Confocal and electron microscopy images of 21 days old nodules embedded in Technovit 8100 and sectioned. **a**–**e** Immunofluorescence assays of Technovit 8100 sections labelled with an LM19 antibody (recognizes un-esterified pectin) from EV (**a**, **b**) and *SyPG1/2-RNAi* (**c**, **d**) transformed nodules ($n \geq 20$ nodules). Green indicates the LM19 signal and magenta indicates the mCherry-tagged *S. meliloti* 2011. Quantification of LM19 fluorescence intensities inside infected cells of control (EV) and RNAi nodules (**e**, $n = 10$ nodules). Fluorescence intensity measurements were performed with Fiji, and graphs were generated with GraphPad Prism 10. Experiments were performed with 3 independent replicates, with a minimum of 10 nodules in each experiment. Box-whiskers plot with all data points shown; the boxes are extended from the 25th to 75th percentiles and the line in the middle of the box is plotted at the median. Data are mean ± SE. Statistics were performed with an unpaired two-tailed student's *t*-test: $p < 0.0001$. Scale bars = 10 µm. The sketches in (**b**) and (**d**) were generated using Adobe Illustrator. **f**–**i** Immunogold labeling using the antibody LM19 (10 nm) was conducted on infected cells from EV (**f**, **g**) and *SyPG1/2-RNAi* (**h**, **i**) transformed nodules ($n = 3$ nodules), revealing labeling within and around symbiosomes in the *SyPG1/2-RNAi* transformed nodules (indicated by white arrows). **g** and **i** are the magnified views of the areas marked by red boxes in (**f**) and (**h**), respectively. The experiments were performed with 2 independent replicates, with 3 nodules in each experiment. Scale bars = 1 µm in (**f**, **h**) and 0.5 µm in (**g**, **i**).

immunofluorescence data, almost no gold particles were observed around the symbiosome in control nodules indicating the absence of de-methylesterified pectins in the symbiosome space (Fig. 4g). By contrast, a substantial accumulation of gold particles was found in the symbiosome spaces of nodules from *SyPG1/2-RNAi* transformed roots (Fig. 4i). In addition, we also detected methylesterified pectin using the LM20 antibody, which showed no significant difference in the infected cells of control nodules and *SyPG1/2-RNAi* nodules (Supplementary Fig. 12). Performing these immunofluorescence assays on *SyPG1/2-Cas9* transformed nodules, confirmed the same patterns that we observed on *SyPG1/2-RNAi* nodules (Supplementary Fig. 13). These data clearly indicate that the symbiosome space is continuously cleared from de-esterified pectins by the action of SyPG1/2.

Un-esterified pectin impairs the growth of rhizobia

To understand the positive function of SyPG1 and SyPG2 for symbiosome function, we assessed the direct impact of pectins on rhizobia. Polygalacturonic acids (PGAs) are un-esterified HGs that can be broken down into short-chain oligogalacturonic acids (OGs) in the presence of PGs. Thus, we investigated the effect of PGA on the growth of rhizobia. For this, we cultured *S. meliloti* 2011 in the presence of different concentrations of PGA and measured bacterial growth over a period of 10 h. Indeed, first inhibitory effects of PGA on bacterial growth were observed at a concentration of 0.5‰ with a strong inhibition occurring at 1‰ (Fig. 5a). These results were also recapitulated in bacterial growth assay on solid TY plates (Fig. 5b).

We then examined the effect of PGA on rhizobial cell integrity using a "live/dead" staining. In this assay, we visualized bacterial cells using SYTO9 and counterstained with propidium iodide (PI) at pH 5.0 that resembles the acidic environment of the symbiosome in *M. truncatula* nodules, which has been described to be between pH 4.5–5.0[19]. While living cells are unable to take up PI, the stain is incorporated into dead cells turning them fluorescent. While most cells were only stained by SYTO9 in the control condition, PGA treatment of rhizobia resulted in high numbers of dead cells with more than 35% of the cells being stained by PI (magenta, Fig. 5c–e and Supplementary Fig. 14). This effect of PGA on rhizobia was also confirmed by using scanning electron microscopy (SEM). Here, significantly more rhizobia were damaged and showed ruffled surfaces after PGA treatment compared to the control (59/113 *vs* 3/107; Fig. 5f, g). In addition, we also investigated the effect of GalA2, a short-chain OG possibly produced during the degradation of PGA by PGs[20], on rhizobial growth. Here, no effect of GalA2 (2‰) on rhizobial survival was observed (Supplementary Fig. 15a–d). Given the morphological and physiological differences between free-living bacteria and differentiated bacteroids within symbiosomes, we directly applied PGA and GalA2 onto nodule sections. As shown in Fig. 5h–k and Supplementary Fig. 15e–g, the activity of bacteroids experienced a significant reduction subsequent to PGA

https://doi.org/10.1038/s41467-025-67404-1

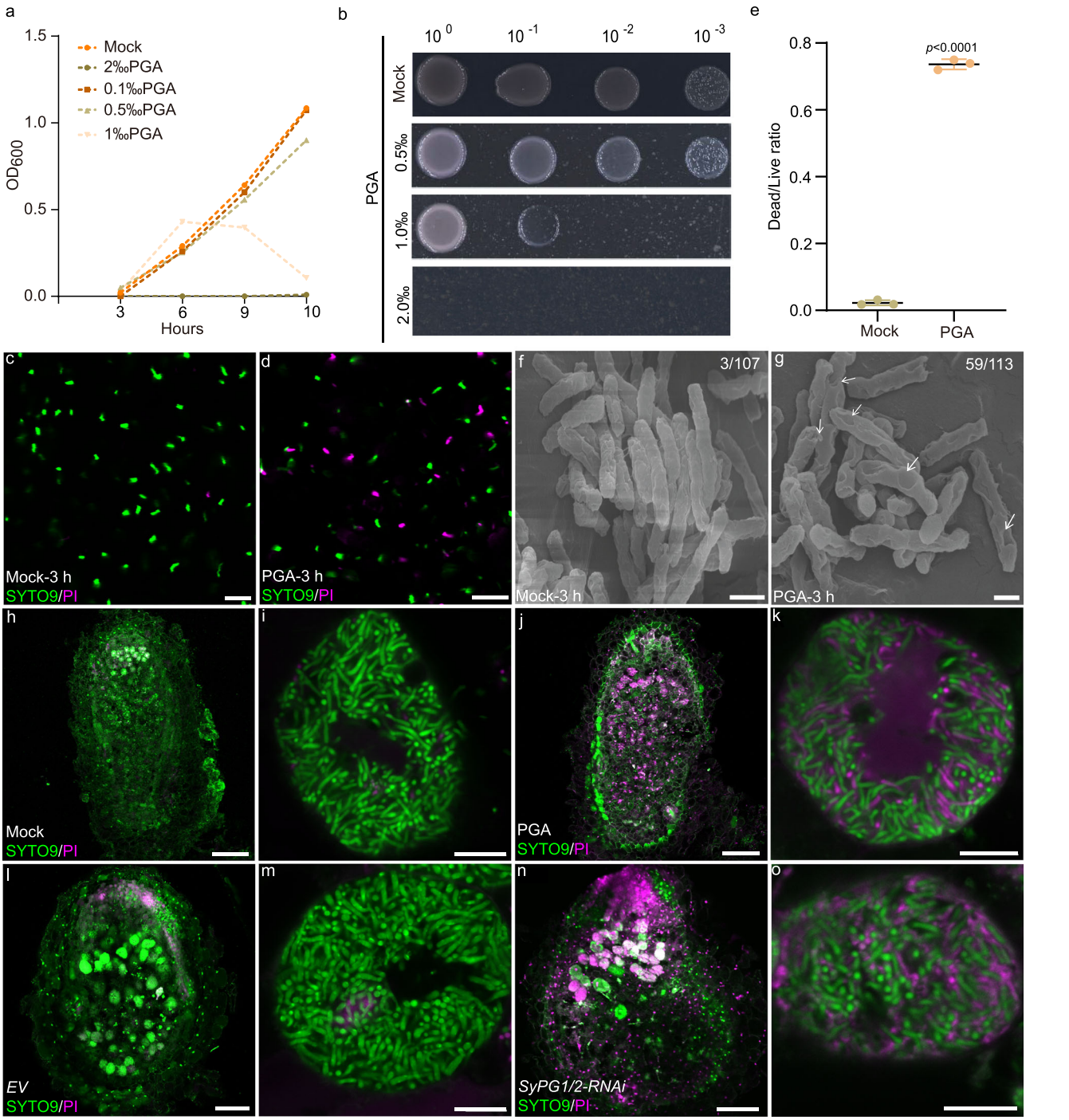

Fig. 5 | Un-esterified pectins inhibit rhizobial growth. a, **b** Growth inhibitory effects of different concentrations of un-esterified pectin (PGA) on rhizobial growth in liquid (**a**) and solid (**b**) TY media. **c**–**g** The inhibitory activity of PGA on rhizobia as well as cell integrity was further confirmed by "live/dead" staining using SYTO9/PI (**c**–**e**) and scanning electron microscopy (SEM, **f**, **g**). Green indicates the rhizobia stained with SYTO9 and magenta indicates the dead rhizobia stained with PI in (**c**, **d**). **a**, **e** were generated using GraphPad Prism 10. The error bars (in **e**) indicate the mean value ± the standard deviation (SD). All experiments were repeated with 3 independent experiments, and statistics were performed using an unpaired two-tailed student's *t*-test: $p < 0.0001$ (**e**). Arrows in (**g**) indicate areas of the rhizobial surface damaged by the PGA treatment. The SEM experiment was performed with 2 independent experiments. Scale bars = 10 μm in (**c**, **d**) and 0.5 μm in (**f**, **g**). **h**–**k** Nodule sections were used for live/dead staining after mock (**h**, **i**) and PGA treatment (**j**, **k**) ($n \geq 30$ nodules) on 21 days old nodules. Data were performed with 3 independent experiments, and at least 30 nodules in each experiment were analyzed. **l**–**o** Nodule sections from EV (**l**, **m**) and *SyPG1/2-RNAi* (**n**, **o**) transformed nodules were used for live/dead staining ($n \geq 20$ nodules). Data were performed with 2 independent experiments, with at least 20 nodules in each experiment. Scale bars = 100 μm in (**h**, **j**), 50 μm in (**l**, **n**), 10 μm in (**i**, **k**, **m**, **o**).

treatments, whereas it remained unaffected by GalA2 treatment. Moreover, we directly assessed the activity of bacteroids in nodules transformed with EV, *SyPG1/2-RNAi*, and *SyPG1/2-Cas9*. The results were in line with those of our in vitro assays, showing that the activity of bacteroids in *SyPG1/2-RNAi* and *SyPG1/2-Cas9* transformed nodules was severely impaired (Fig. 5i–o and Supplementary Fig. 16). Altogether, those results indicate that un-esterified pectins have a negative effect on the activity of bacteria.

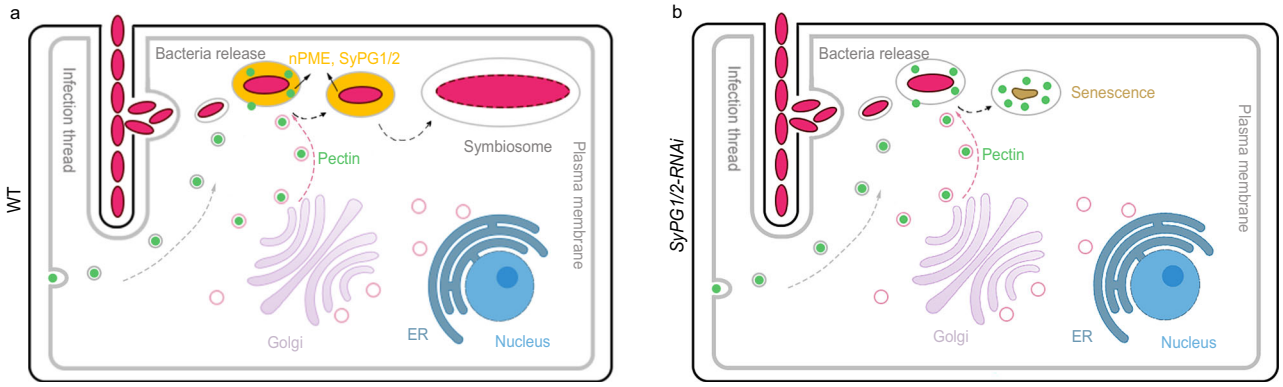

Fig. 6 | Working model for SyPG1 and SyPG2 function. a nPME, SyPG1, and SyPG2 are located in the symbiosome space continuously degrade pectins delivered to the symbiosome to maintain a pectin-free zone to ensure rhizobial growth. **b** In *SyPG1/2-RNAi* nodules, the secreted pectin cannot be degraded, leading to an accumulation of unesterified pectins, which in turn affects growth of rhizobia within the symbiosome. The gray dashed arrow and pink dashed arrow indicate two possible pathways for pectin deposition to the symbiosome space. The sketches were generated using Adobe Photoshop.

Discussion

Symbiosomes are the fundamental units for nitrogen fixation in legume nodules. Although the symbiosome space resembles an apoplastic compartment, it is well accepted that these structures lack typical plant cell wall components. However, how this cell wall free environment is been generated or maintained has remained enigmatic. Here, we provide compelling evidence that the symbiosome space remains devoid of cell wall structures through continuous degradation of HGs that are secreted to the symbiosome space. Certain cell wall materials, including HGs, can still be transported to the newly formed symbiosome. To mitigate the negative effects of HGs on bacteroids, the plant secretes SyPG1 and SyPG2 into the symbiosome space to eliminate them (Fig. 6a). Conversely, if the function of SyPG1/2 is silenced, it will result in the excessive accumulation of un-esterified pectin in the symbiosome containing cells, leading to early nodule senescence (Fig. 6b).

We revealed that dynamic pectin modifications occur within the symbiosome space, facilitated by symbiosome-specific cell wall degrading enzymes. Several lines of evidence support this conclusion. First, the expression of *SyPG1* and *SyPG2*, was specifically induced upon rhizobia inoculation (Supplementary Figs. 4a and 5). Second, the subcellular localization reveals that both SyPGs, as well as a nPME, are localized to the symbiosome space (Figs. 1a–d and 2). Third, knockdown the expression of *SyPG1/2* via RNAi or edited *SyPG1/2* by CRISPR-Cas9 all lead to the accumulation of pectin within the symbiosome space, as shown by immunofluorescence labeling and inmuno-gold labeling (Fig. 4 and Supplementary Fig. 13a–e). Finally, unesterified pectins appear to negatively affect bacterial activity within the symbiosome (Fig. 5h–o and Supplementary Figs. 15e–g and 16), suggesting that their clearance is essential for proper symbiotic function. Taken together, these results indicate that SyPG1/2 play a crucial role in degrading pectin to maintain a cell wall–free environment conducive to nitrogen fixation. Notably, rhizobia can survive within the IT, which is directly surrounded by the cell wall, and we also observed that the treatment with PGA had a relatively weaker influence on the rhizobia activity within IT in comparison to the released ones (Supplementary Fig. 17). One possible explanation is that the matrix inside the IT potentially shields them from unesterified pectin, but this hypothesis remains to be verified.

Interestingly, the cell wall component clearing phenomenon may not be limited to pectin. It has recently been shown that the *M. truncatula* Glycoside Hydrolase 9C2 (GH9C2) is required for cell wall degradation in primary ITs and around bacterial release sites (infection droplets). Upon symbiosome formation, GH9C2 remained associated with symbiosomes and co-localized with calcofluor-positive foci[21]. Moreover, proteomic analyses of SMs in *Glycine max* (soybean)[22] and *Lotus japonicus*[23] have identified additional cell wall–modifying enzymes (*e.g.*, Glycosyl hydrolase), suggesting that this mechanism may be conserved across different legume species.

Of note, SyPG1 was also found to localize to ITs and infection droplets (Supplementary Fig. 6a, b), indicating potential involvement in IT growth and bacterial release. However, we did not observe clear defects in IT growth or bacterial release in *SyPG1/2-RNAi* plants, possibly due to functional redundancy among PG family members, as some *PGs* are also upregulated during early stages of infection[24,25].

Our data clearly show that pectins accumulate in the symbiosome space in the absence of SyPG1/2 activity (Fig. 4 and Supplementary Fig. 13a–e). This leaves the questions whether pectins are already enclosed by the SM during bacterial release, or whether they are indeed constantly secreted into the space and then degraded. The first possibility seems unlikely, only minimal pectin signal was observed at infection droplets[26]. In contrast, exocytotic vesicles containing de-methylesterified pectins were observed in the cytosol of infected cells[26], indicating that most likely the pectins were synthesized in infected cells and delivered to the symbiosome spaces. In addition, Gavrin et al. (2016) has also shown that there are endosome-like vesicles containing unesterified pectins in infected cells of soybean nodules[26]. Therefore, the possibility that endocytosed unesterified pectins are re-targeted to the symbiosome cannot be excluded.

In summary, our study reveals a dynamic and targeted degradation of pectins within the symbiosome space, mediated by SyPG1/2. This mechanism ensures a cell wall–free environment necessary for efficient nitrogen fixation. In future, investigate the origin of these pectins and how those enzymes been targeted to symbiosome space and how the bacterial been protected with in IT will offers new insights into understanding the interaction between legume and rhizobia.

Methods

Constructs design

For subcellular localization: the coding sequence of *nPME* (*Medtr2g105560*), *SyPG1* (*Medtr2g032710*) and *SyPG2* (*Medtr6g028080*) were synthesized and then cloned into the GoldenGate EC50507 vector[27], and *Lotus* ubiquitin (Ubi) promoter was used to drive the expression of those genes. For promoter activation: promoter sequences (2000 bp) of *SyPG1* and *SyPG2* were amplified by PCR from *M. truncatula* A17 genomic DNA and then ligated into the pCAMBIA1391 vector by Gibson assembly. For RNAi: the sequence was amplified and cloned into pZHY930 vector by Gibson assembly. For CRISPR gene

editing, the amplified sequences were cloned into pGES402 vector via *Bsa*I enzyme sites[28]. All primers used are listed in Supplementary Table 1.

Hairy root transformation

The constructs were transformed into the *Agrobacterium rhizogenes* (strR, CamR) ArQual strain and used for hairy root transformation as described previously[29]. In short, *M. truncatula* A17 seeds were surface-sterilized by sulfuric acid (10 min) and bleach solution (1.2% sodium hypochlorite, 0.1% sodium dodecyl sulfate; 60 s), with 5 times sterile water rinses between the two steps. Seeds were rinsed five additional times with sterile water before being plated on 1% agar plates and stratified at 4 °C for 3 days. Subsequently, they were germinated overnight at 24 °C in darkness and used for hairy root transformation. After transformation, the plants were kept in darkness at 24 °C for 3 days and then in light at 24 °C for 4 days (upper part of the plate only). Seedlings were then transferred to new Fahräeus medium plates (containing 0.5 mM NH_4NO_3) for an additional 10–14 days, and then positively transformed plants were identified with a portable fluorescent lamp (LUYOR-3415, American Router). The positive composite plants were then transferred to open pots (3:1 mix of vermiculite and perlite, 1 plant/pot) and grown in a greenhouse (12 h light/12 h dark, 25 °C, light intensity 200 µmol/m²/s). Five days later, *S. meliloti* 2011 (OD600 = 0.03; 10 mL/plant) was used to inoculate the plants. Plants were harvested at 3 weeks post-inoculation for further analysis.

Technovit 8100 sectioning and Immunofluorescence

Nodules (3 wpi) were harvested and then immediately fixed in a PBS solution containing 4% paraformaldehyde (PFA) under vacuum for 15 min (twice) and stored at 4 °C in the fixative solution overnight. They were then dehydrated in acetone/H_2O graded series (50%, 70%, 80%, 90%, 100%, 1 h each at 4 °C). Final dehydration in absolute acetone was repeated once, followed by incubation in acetone/Technovit infiltration solution (1:3, 2:2, 3:1, 60 min each at 4 °C), and then the final infiltration in pure Technovit infiltration solution was carried out overnight at 4 °C. Embedding of the samples was performed as directed by the manufacturer. Nodule sections (10 µm) for immunofluorescence labeling were obtained using a RM2155 microtome (Leica). The nodule sections were blocked with 3% BSA for 30 min at room temperature. Then the primary antibody (LM19 (2w00019S) and LM20 (2w00020s), from Abmart) was applied to the sections (1 to 50 diluted in PBS solution supplied with 3% BSA) and incubated for 1–2 h at room temperature. The sample was then washed at least 3 times (5 min each time) with PBS solution. The secondary antibody (conjugated with Alex Fluor 488 (A-11006), from Invitrogen) was then added diluted in PBS solution containing 3% BSA and then the sample was incubated for another 30 min to 1 h. The sample was then washed at least 3 times before images were taken. Note that after applying the secondary antibody all steps were performed in darkness. The samples were then imaged using a Leica SP8 confocal microscope.

For immuno-gold staining: the samples were embedded with LR White according to the protocol descript in Su et al.[11]. Goat-anti Rat IgG 10 nm gold conjugated polyclonal antibody (Sigma, G7035) was used as secondary antibody.

Technovit 7100 sections and GUS staining

The sample preparation followed same process described above for Technovit 8100, except that ethanol was used instead of acetone. The GUS staining was performed according to a previous study[30]. Briefly, tissue samples were collected in 5 mL tubes immersed in GUS staining solution, following vacuum twice for 10 min each time. The samples were incubated at 37 °C for 4–8 h (in dark). After staining, the samples were cleared with 75% ethanol and stored in 75% ethanol for subsequent analysis. The stained nodules were embedded in Technovit 7100 for sectioning and visualization. All nodule sections were stained with 0.05% w/v Toluidine Blue or 0.1% w/v Ruthenium red prior to imaging. Images were taken with a ZEISS Axiolab 5 microscope.

In situ hybridization

Using specific primers (see Supplementary Table 1), the 254 bp sequence fragment of *SyPG1* (corresponding to part of the coding sequence and the 3′ untranslated region) and the 251 bp coding sequence fragment of *SyPG2* were amplified from cDNA using KOD polymerase (KFX-101, Stratagene, San Diego, CA). Subsequently, the amplified fragments were cloned into the pEASY®-Blunt3 vector (CB301-01, TransGen Biotech, San Diego, CA). Digoxigenin-labelled sense or antisense probes were synthesized using T7 or SP6 RNA polymerase. *Medicago* nodule samples were collected 7–10 days and 21 days post-inoculation. Following fixation in 4% PFA, the samples underwent paraffin embedding and sectioning at 8–10 µm thickness. After deparaffinization and dehydration, sections were subjected to hybridization staining according to previously described method[31].

Localization analysis

14 days old nodules were embedded in 3% agarose and cut into 70 µm sections using a vibratome (VT1000S, Leica). FM4-64 (5 µg ml^{-1}, from Sigma, F34653) was used to stain the membrane. The cell wall structure was stained with Calcofluor White M2R (0.1%, from Sigma, 910090). Images were acquired with a Leica SP8 confocal microscope with a 63×/1.2 (HC PL APO CS2) water immersion objective and an argon Light Laser (DAPI: 405 nm (ex)/415–465 nm; GFP: 488 nm (ex)/500–550 nm (em); mCherry: 561 nm (ex)/575–630 nm). All the image analyses and projections were performed using either the Fiji[32] or Imaris software.

RNA extraction and quantitative real-time PCR

Total RNA was extracted using the Trizol reagent kit (Aidlab Biotechnologies Co., Ltd). The cDNA was synthesized using Hifair II 1st Strand cDNA Synthesis SuperMix (Yeasen Biotech, Shanghai, China). Quantitative real-time PCR (qRT-PCR) was accomplished using Hieff® qPCR SYBR Green Master Mix (No Rox) and CFX Connect real-time PCR detection system (Bio-Rad). The relative expression level was calculated by $2^{-\Delta\Delta Ct}$ (ΔΔCt is the difference of ΔCt between the experimental group and the control group). *PP2A* was used as the reference gene[33]. All primers used are listed in Supplementary Table 1.

PGA treatment

For the PGA (Sigma, P3889) treatment *S. meliloti* 2011 were grown in TY liquid medium at 28 °C to OD600 = 1.0, and then 1:100 added to the TY liquid medium containing different doses of PGA (0.1‰, 0.5‰, 1‰ and 2‰). The rhizobia were then incubated at 28 °C and the OD600 was measured every 3 h with a spectrophotometer (Eppendorf BioPhotometer D30). For testing *S. meliloti* 2011 growth on PGA-containing solid plates the *S. meliloti* 2011 was cultured in TY liquid medium until it reached an OD600 = 1.0, then 10 µL of a dilution series was plated onto TY solid medium containing different concentrations of PGA and incubated at 28 °C for 3–4 days. 2‰ PGA was used to treat the rhizobia for scanning electron microscopy analysis.

Scanning electron microscope analysis

Rhizobia were grown overnight in TY liquid medium, then diluted into fresh TY liquid medium with or without PGA (2‰, OD600 = 0.2) culture for 3 h. The rhizobia were then pelleted by centrifugation (1000 × *g*, 10 min) and washed with 0.01 M PBS buffer (pH 7.0). Immediately after washing, the rhizobia were placed in Formalin-Aceto-Alcohol (from Servicebio, G1103) fixative at 4 °C overnight. The overnight fixed samples were dehydrated sequentially for 15–20 min in ethanol solutions of different concentrations (30%, 50%, 70%, 85%, 95%, and 100%), then the dehydrated samples were freeze-dried using

a Labogene Scanvac CoolSafe 110-4. Finally, the samples were examined using a scanning electron microscope (FE-SEM, SU8010, HITACHI, Japan).

Live/dead staining

The rhizobia live/dead staining was carried out with solution containing SYTO9 (1:100; from Thermo Fisher, S34854) and PI (1:100, from Solarbio, C0080) in PBS (0.01 M, pH 7.0) for 1–5 min at room temperature. Regarding the nodule sections, the nodules (3 weeks post-inoculation) from the transformed roots of EV, *SyPG1/2-RNAi*, and *SyPG1/2-Cas9* were embedded in 3% agarose. After that, vibratome sections with a thickness of 70 µm were obtained. Immediately, these sections were stained using live/dead staining for 5 min before undergoing microscopy imaging. For PGA and GalA2 treatments: The vibratome sections obtained from wild-type samples were immediately treated with PGA (2‰, from Sigma, P3889) and GalA2 (2, from Macklin, D981325) at room temperature for 3 h before performing live/dead staining for image acquisition. The results were observed using a Leica SP8 confocal microscope as described above.

Statistical analysis

The data were analysed using GraphPad Prism 10 built-in statistical tools.

Reporting summary

Further information on research design is available in the Nature Portfolio Reporting Summary linked to this article.

Data availability

All the data are included in the article and/or SI Appendix. Source data are provided with this paper.

References

1. Gigli-Bisceglia, N., Engelsdorf, T. & Hamann, T. Plant cell wall integrity maintenance in model plants and crop species-relevant cell wall components and underlying guiding principles. *CMLS* **77**, 2049–2077 (2020).
2. Yapo, B. M. Pectic substances: from simple pectic polysaccharides to complex pectins-A new hypothetical model. *Carbohydr. Polym.* **86**, 373–385 (2011).
3. Yang, Y. & Anderson, C. T. Biosynthesis, Localisation, and Function of Pectins in Plants. In Pectin: Technological and Physiological Properties (Kontogiorgos, V. ed.) https://doi.org/10.1007/978-3-030-53421-9_1. (Springer, Cham, 2020).
4. Jolie, R. P., Duvetter, T., Van Loey, A. M. & Hendrickx, M. E. Pectin methylesterase and its proteinaceous inhibitor: a review. *Carbohydr. Res.* **345**, 2583–2595 (2010).
5. Kumar, R. et al. Sequence, structure and functionality of pectin methylesterases and their use in sustainable carbohydrate bioproducts: a review. *Int. J. Biol. Macromol.* **244**, 125385 (2023).
6. Anderson, C. T. & Pelloux, J. The dynamics, degradation, and afterlives of pectins: influences on cell wall assembly and structure, plant development and physiology, agronomy, and biotechnology. *Annu. Rev. Plant Biol.* **76**, 85–113 (2025).
7. Rich, M. K., Schorderet, M. & Reinhardt, D. The role of the cell wall compartment in mutualistic symbioses of plants. *Front. Plant Sci.* **5**, 238 (2014).
8. Gage, D. J. Infection and invasion of roots by symbiotic, nitrogen-fixing rhizobia during nodulation of temperate legumes. *Microbiol. Mol. Biol. Rev.* **68**, 280–300 (2004).
9. Zhang, G. F. & Ott, T. Cellular morphodynamics and signaling around the transcellular passage cleft during rhizobial infections of legume roots. *Curr. Opin. Cell Biol.* **91**, 102436 (2024).
10. Su, C. et al. Stabilization of membrane topologies by proteinaceous remorin scaffolds. *Nat. Commun.* **14**, 323 (2023).
11. Su, C. et al. Transcellular progression of infection threads in *Medicago truncatula* roots is associated with locally confined cell wall modifications. *Curr. Biol.* **33**, 533–542 (2023).
12. Brewin, N. J. Plant cell wall remodelling in the rhizobium–legume symbiosis. *Crit. Rev. Plant Sci.* **23**, 293–316 (2004).
13. Brewin, N. J. et al. Bacterial and plant glycoconjugates at the rhizobium-legume interface. *Biochem. Soc. Symp.* **60**, 61–73 (1994).
14. Redondo-Nieto, M., Pulido, L., Reguera, M., Bonilla, I. & Bolaños, L. Developmentally regulated membrane glycoproteins sharing antigenicity with rhamnogalacturonan II are not detected in nodulated boron deficient *Pisum sativum*. *Plant Cell Environ.* **30**, 1436–1443 (2007).
15. Roux, B. et al. An integrated analysis of plant and bacterial gene expression in symbiotic root nodules using laser-capture microdissection coupled to RNA sequencing. *Plant J.* **77**, 817–837 (2014).
16. Schiessl, K. et al. Nodule inception recruits the lateral root developmental program for symbiotic nodule organogenesis in *Medicago truncatula*. *Curr. Biol.* **29**, 3657–3668 (2019).
17. Mahmood, U. et al. Comprehensive analysis of polygalacturonase genes offers new insights into their origin and functional evolution in land plants. *Genomics* **113**, 1096–1108 (2021).
18. Jardinaud, M. F., Carrere, S., Gourion, B. & Gamas, P. Symbiotic nodule development and efficiency in the *Medicago truncatula Mtefd*-1 mutant is highly dependent on sinorhizobium strains. *Plant Cell Physiol.* **64**, 27–42 (2023).
19. Pierre, O. et al. Peribacteroid space acidification: a marker of mature bacteroid functioning in *Medicago truncatula* nodules. *Plant Cell Environ.* **36**, 2059–2070 (2013).
20. Safran, J. et al. Plant polygalacturonase structures specify enzyme dynamics and processivities to fine-tune cell wall pectins. *Plant Cell* **35**, 3073–3091 (2023).
21. Zhao, L., Ji, C. Y., Murray, J. D. & Liu, C. W. A legume cellulase required for rhizobial infection and colonization in root nodule symbiosis. *Nat. Commun.* **16**, 6663 (2025).
22. Clarke, V. C. et al. Proteomic analysis of the soybean symbiosome identifies new symbiotic proteins. *Mol. Cell Proteom.* **14**, 1301–1322 (2015).
23. Wienkoop, S. & Saalbach, G. Proteome analysis. Novel proteins identified at the peribacteroid membrane from *Lotus japonicus* root nodules. *Plant Physiol.* **131**, 1080–1090 (2003).
24. Carrere, S., Verdier, J. & Gamas, P. MtExpress, a comprehensive and curated RNAseq-based gene expression atlas for the model legume *Medicago truncatula*. *Plant Cell Physiol.* **62**, 1494–1500 (2021).
25. Muñoz, J. A. et al. MsPG3, a *Medicago sativa* polygalacturonase gene expressed during the alfalfa-rhizobium meliloti interaction. *Proc. Natl. Acad. Sci. USA* **95**, 9687–9692 (1998).
26. Gavrin, A. et al. VAMP721a and VAMP721d are important for pectin dynamics and release of bacteria in soybean nodules. *N. Phytol.* **210**, 1011–1021 (2016).
27. Weber, E., Engler, C., Gruetzner, R., Werner, S. & Marillonnet, S. A modular cloning system for standardized assembly of multigene constructs. *PLoS ONE* **6**, e16765 (2011).
28. Bai, M. et al. Combination of two multiplex genome-edited soybean varieties enables customization of protein functional properties. *Mol. Plant* **15**, 1081–1083 (2022).
29. Boisson-Dernier, A. et al. Agrobacterium rhizogenes-transformed roots of *Medicago truncatula* for the study of nitrogen-fixing and endomycorrhizal symbiotic associations. *Mol. Plant Microbe Interact.* **14**, 695–700 (2001).
30. Su, C. et al. The *Medicago truncatula* DREPP protein triggers microtubule fragmentation in membrane nanodomains during symbiotic infections. *Plant Cell* **32**, 1689–1702 (2020).
31. Jackson, A. C. Detection of rabies virus mRNA in mouse brain by using in situ hybridization with digoxigenin-labelled RNA probes. *Mol. Cell Probes* **6**, 131–136 (1992).

32. Schindelin, J. et al. Fiji: an open-source platform for biological-image analysis. *Nat. Methods* **9**, 676–682 (2012).
33. Kakar, K. et al. A community resource for high-throughput quantitative RT-PCR analysis of transcription factor gene expression in *Medicago truncatula*. *Plant Methods* **4**, 18 (2008).

Acknowledgements

We thank Dr. Jinxia Yun (Lanzhou University) for seeds and the entire soybean group (Huazhong Agricultural University) for the discussions on the project. We would also like to thank Prof. Jeremy Murray (the Centre of Excellence Plant and Microbial Sciences, CEPAMS), Prof. Ertao Wang (the Centre of Excellence Plant and Microbial Sciences, CEPAMS) and Prof. Chengwu Liu (University of Science and Technology of China) for their valuable comments and suggestions on the manuscript, and Dr. Prof. Yuefeng Guan of Guangzhou University for provide the pGES402 vector. This work was supported by: Biological Breeding-National Science and Technology Major Project (2024ZD04079 to X.L.); National Natural Science Foundation of China (32570289 and 301/590224002 to C.S.); Engineering Nitrogen Symbiosis for Africa (ENSA) project currently supported through a grant to the University of Cambridge by the Bill & Melinda Gates Foundation (OPP1172165 to T.O.).

Author contributions

Conceptualization: C.S., X.L., T.O.; Investigation: Y.G., L.C., W.Y., T.Y., Q.L., K.C., J.Y., C.S.; Writing–original draft: C.S.; Writing–review & editing: Y.G., L.C., W.Y., T.Y., Q.L., K.C., J.Y., T.O., X.L., C.S.

Competing interests

The authors declare no competing interests.

Additional information

Supplementary information The online version contains supplementary material available at https://doi.org/10.1038/s41467-025-67404-1.

Correspondence and requests for materials should be addressed to Thomas Ott or Chao Su.

Peer review information *Nature Communications* thanks the anonymous reviewer(s) for their contribution to the peer review of this work. A peer review file is available.